Published in final edited form as:
Cell Metab. 2012 April 4; 15(4): 492–504. doi:10.1016/j.cmet.2012.03.010.

Wnt signaling activation in adipose progenitors promotes insulin-independent muscle glucose uptake

Daniel Zeve[1,#], **Jin Seo**[1,#], **Jae Myoung Suh**[1,#], **Drew Stenesen**[1], **Wei Tang**[1], **Eric D. Berglund**[2], **Yihong Wan**[3], **Linda J. Williams**[1], **Ajin Lim**[1], **Myrna J. Martinez**[1], **Renée M. McKay**[1], **Douglas P. Millay**[4], **Eric N. Olson**[4], and **Jonathan M. Graff**[1,4,*]

[1]Department of Developmental Biology, University of Texas Southwestern Medical Center, 6000 Harry Hines Blvd., NB5.118, Dallas, Texas 75390-9133, USA

[2]Department of Internal Medicine, University of Texas Southwestern Medical Center, 6000 Harry Hines Blvd., NB5.118, Dallas, Texas 75390-9133, USA

[3]Department of Pharmacology, University of Texas Southwestern Medical Center, 6000 Harry Hines Blvd., NB5.118, Dallas, Texas 75390-9133, USA

[4]Department of Molecular Biology, University of Texas Southwestern Medical Center, 6000 Harry Hines Blvd., NB5.118, Dallas, Texas 75390-9133, USA

SUMMARY

Adipose tissues provide circulating nutrients and hormones. We present *in vivo* mouse studies highlighting roles for Wnt signals in both aspects of metabolism. β-catenin activation in PPARγ–expressing fat progenitors (PBCA) decreased fat mass and induced fibrotic replacement of subcutaneous fat specifically. In spite of lipodystrophy, PBCA mice did not develop the expected diabetes and hepatosteatosis, but rather exhibited improved glucose metabolism and normal insulin sensitivity. Glucose uptake was increased in muscle independently of insulin, associated with cell surface translocation of glucose transporters and AMPK activation. *Ex vivo* assays showed these effects were likely secondary to blood-borne signals since PBCA sera or conditioned media from PBCA fat progenitors enhanced glucose uptake and activated AMPK in muscle cultures. Thus, adipose progenitor Wnt activation dissociates lipodystrophy from dysfunctional metabolism and highlights a fat-muscle endocrine axis, which may represent a potential therapy to lower blood glucose and improve metabolism.

INTRODUCTION

The ability to maintain metabolic homeostasis was a key step during the evolutionary transition to multicellularity and tissue specification. To meet the energy demands of individual cells, organisms have adapted to distribute nutrients through circulatory systems (Strilic et al., 2010). Carbohydrates (e.g., glucose) are a main circulating nutrient to preserve cellular energy balance. Intravascular and intracellular levels of carbohydrates are regulated by conserved, related mechanisms, such as insulin and AMP kinase (AMPK) signaling (Kahn et al., 2005). In addition to mechanistic conservation, evolutionary pressures have

*Correspondence: jon.graff@utsouthwestern.edu.
#All authors contributed equally to this work

maintained homeostasis through dynamic interactions of tissues including neural, muscle, and fat lineages (Galic et al., 2010; Huang and Czech, 2007; Morton et al., 2006).

Muscles are a major source of glucose uptake and utilization. Indeed, insulin resistance and impaired glucose uptake in muscle are hallmarks of Type II diabetes (DeFronzo and Tripathy, 2009; Fujii et al., 2006; Garvey et al., 1998; Zierath et al., 1996). In muscle, insulin and AMPK signaling activate glucose uptake by stimulating translocation of glucose transporters (e.g., Glut4) from the cytoplasm to the plasma membrane (Huang and Czech, 2007; Lemieux et al., 2003; Steinberg and Kemp, 2009).

White adipose tissues also regulate homeostasis as underscored by the metabolic perturbations: dyslipidemia, ectopic fat deposition, insulin resistance, and diabetes, observed in obesity and lipodystrophy (Fiorenza et al., 2010; Garg, 2004; Must et al., 1999; Savage, 2009). Even though adipose tissues plays a pivotal role in metabolism, its cellular lineage and *in vivo* development are just beginning to be elucidated (Zeve et al., 2009). Wnt signaling has been implicated, based upon *in vitro* and transgenic studies, as inhibiting murine fat differentiation (Bennett et al., 2002; Longo et al., 2004; Ross et al., 2000; Wright et al., 2007).

To dissect the Wnt pathway in adipose lineage formation we evaluated canonical, cell autonomous Wnt signaling within murine mature adipocytes and adipose progenitor cells (Rodeheffer et al., 2008; Tang et al., 2011; Tang et al., 2008; Zeve et al., 2009). Using two different drivers, aP2-Cre and PPARγ-tTA; TRE-Cre, we drove expression of a constitutively active form of β-catenin, using a conditional allele of the endogenous locus, at various stages in the adipose lineage. We found that activating Wnt signaling within mature adipocytes with aP2-Cre (termed A-BCA for **A**dipocyte **β**-**C**atenin **A**ctivated) did not change adiposity or metabolism. These results contrast with those produced using the PPARγ-tTA; TRE-Cre driver in which Wnt signaling was altered in the adipose progenitor cells and then throughout the lineage. These mice (termed P-BCA for **P**rogenitor **β**-**C**atenin **A**ctivated) had lipodystrophic levels of fat, hypertriglyceridemia and a paucity of adipocytes. There was a regional specificity to this adipocyte loss; subcutaneous depots had fibrotic replacement, while visceral depots did not. Despite the paucity of adipocytes and evident hypertriglyceridemia, P-BCA mutants were protected from hepatic steatosis, a hallmark of adipose absence (Fiorenza et al., 2010; Garg, 2004). Furthermore, P-BCA mice, in contrast to other forms of lipodystrophy, displayed improved glucose metabolism, with muscles utilizing 2–4 times more glucose than controls. These changes were independent of insulin. Rather, increased glucose uptake was caused tissue non-autonomously with activation of AMPK and translocation of glucose transporters to the cell surface in muscles. The increase in glucose uptake was apparent *ex vivo* immediately after placing P-BCA mutant muscles in culture, but thereafter was reversible, indicating that the increase in glucose uptake was not intrinsic to the muscles. Indeed, mutant sera increased glucose uptake and AMPK activity of cultured muscles, pointing to the presence of a humoral factor. A similar activity was also present in conditioned media of P-BCA mutant adipose stromal vascular (SV) cells, in which adipose progenitors reside, supporting the idea that altered adipose progenitors may be the source of the signal. Thus, the P-BCA model illuminates a possible therapeutic method to improve metabolism in the face of adipose dysfunction and diabetes.

RESULTS

Mice with β-Catenin Activated in Mature Adipocytes Have Normal Metabolism

MacDougald and colleagues reported that transgenic expression of the secreted Wnt10b ligand from mature adipocytes using the FABP4/aP2 promoter resulted in an ~50% decrease

in total body fat (Longo et al., 2004). To examine cell-autonomous canonical Wnt in mature adipocytes, we crossed our described aP2-Cre mice (Figure 1A) (Tang et al., 2008) with a conditional allele of β-catenin (fBC for floxed β-catenin) in which Cre expression activates Wnt signaling, generating aP2-Cre; fBC (A-BCA for **A**dipocyte **β**-**C**atenin **A**ctivated) mice. Previous studies, and confirmed here, showed that this Cre is highly expressed in mature adipocytes, but not in adipose progenitors (Figure S1A, S1B, S2C, S2D) (Tang et al., 2011; Tang et al., 2008; Zeve et al., 2009). Westerm blots indicated aP2-Cre; fBC combination was effective, the activated, faster migrating form of β-catenin was detected in adipose depots of A-BCA mutant, but not control, adipose tissues (Figure 1B). To further examine effectiveness and specificity, we performed qPCR of the floated adipocyte fraction and the stromal vascular fraction (SVF), which contains adipose progenitors. We found increased Wnt target gene expression in the floated adipocyte fraction adipocytes of A-BCA mice, but not in their stromal vascular fraction (SVF), containing adipose progenitors (Figure 1C).

4-month old A-BCA mutant mice fed normal chow had no discernable subcutaneous or visceral adipose or metabolic phenotypes (Figure 1). Controls and A-BCA mutants had equal amounts of fat based upon Magnetic Resonance Imaging (MRI) scans, Nuclear Magnetic Resonance (NMR) fat content analyses, and adipose depot weight, size and morphology (Figure 1D-1G). Histological analyses of the inguinal (IGW) and perigonadal (PGW) adipose depots revealed no apparent changes (Figure 1H). We did detect fibrosis in subdermal tissue (Figure 1I) similar to previous data of cell non-autonomous Wnt activation models in which expression of Wnt10b is driven by aP2 (Longo et al., 2004). The size and morphology of other organs such as heart and kidney were unchanged (Figure S1C, not shown). Serum analysis showed no significant difference in adiponectin, leptin, triglyceride (TG), or insulin levels (Figure 1J and 1K). Fed and fasted blood glucose levels and glucose tolerance tests (GTTs) were unaltered (Figure 1L and 1M). Notably, the normalcy is dissimilar from previous data of cell non-autonomous Wnt activation models in which expression of Wnt10b driven by aP2 resulted in an approximately 50% reduction in subcutaneous and visceral fat (Longo et al., 2004; Wright et al., 2007). The differences of the two murine phenotypes may derive from the secretory nature of Wnt10b and its possible effects on other cell types present in adipose tissue such as endothelial cells and adipose progenitor cells, or cells affected at a distance.

Mice with β-Catenin Activation in the Progenitor Compartment Have Severe Loss of Adiposity

We next examined the effects of cell autonomous Wnt pathway activation in adipose progenitor cells (Figure 2). For this, we turned to a strain, PPARγ-tTA; TRE-Cre, in which Cre is expressed in adipose lineage cells (Figure S2A-S2C) (Tang et al., 2011; Tang et al., 2008; Zeve et al., 2009). Unexpectantly, Cre is expressed in similar levels between SV cells and mature adipocytes, possibly because tTA is saturating, inducing maximal Cre expression in the trigenic system (Figure S2C) (El-Bizri et al., 2008; Sakahara et al., 2009). Of note, the aP2 driver expresses 200 times more Cre than the PPARγ trigenic system driver in mature adipocytes (Figure S2D). We crossed this combination with the aforementioned floxed β-catenin allele to generate PPARγ-tTA; TRE-Cre; fBC (P-BCAfor **P**rogenitor **β**-**C**atenin **A**ctivated) mice (Figure 2A). Western blots indicated that the P-BCA genetic arrangement was effective; the faster migrating activated form of β-catenin was present in mutant, but not control (PPARγ-tTA; TRE-Cre or PPARγ-tTA; fBC), adipose tissue, and also not in other tissues (Figure 2B and 2C).

We next examined 3.5–4.5 month old P-BCA mice for possible adipose phenotypes; sibling controls contained the PPARγ-tTA allele, as well as either TRE-Cre or fBC (PPARγ-tTA; TRE-Cre or PPARγ-tTA; fBC). P-BCA mice had markedly reduced fat (Figure 2D-2H). MRI scans indicated absence of subcutaneous (SQ) white adipose tissue accompanied by a

dramatic reduction of visceral depots (Figure 2D). NMR fat content analyses showed a > 80% fat reduction, similar to that seen in 4-month old PPARγ null mice (Figure 2E). These PPARγ null mice contain a PPARγ-tTA null allele, a PPARγ floxed allele, and Sox2-Cre; the latter expresses Cre in the epiblast, deleting PPARγ in embryos and mice but not in extra-embryonic tissues (Hayashi et al., 2002). These PPARγ null mice were created in a similar fashion, and have a similar lipodystrophic phenotype, to the mice described by Mortensen and colleagues (Duan et al., 2007). P-BCA adiponectin levels were undetectable and leptin levels were ~1% of controls (Figure 2F). Explanted P-BCA visceral fat was significantly small (Figure 2G and 2H). However, in contrast to the MRI and NMR analyses indicating absence of SQ fat (Figure 2D and 2E), the SQ depots were of the same size and weight as controls (Figure 2G and 2H). The size of other organs, for example, kidney and heart, were unchanged (Figure S2E, not shown).

Progenitor β-Catenin Activation Appears to Induce a Fate Change

The results of the MRI and NMR studies, showing a marked fat reduction, and the normal size and weight of the SQ adipose depots were discordant. This difference was also evident upon palpation, which indicated that although the P-BCA SQ depots had appropriate morphology, they did not have normal adipose texture; rather they were hard and rubbery. P-BCA SQ depots had increased density, sinking in water (Figure 3A). P-BCA inguinal (IGW) adipose tissue showed dense, eosin-positive fibers that had the appearance of collagen (Figure 3B). Brown adipose tissue was either absent or contained small fibrotic remnants (Figure S3A). The few remaining visceral P-BCA adipocytes were hypertrophied, potentially due to increased demand for lipid storage (Figure 3B). Trichrome collagen staining showed fibrotic SQ and subdermal adipose depots, and almost no adipocytes (Figure 3C and S3B). P-BCA IGW had reduced expression of adipocyte lineage genes (e.g., PPARγ, leptin), and expression of fibroblast markers (e.g., DDR2, Fsp-1) and β-catenin targets (e.g., Wisp2) (Figure 3D and 3E). Although P-BCA perigonadal (PGW) adipose tissue had increased expression of β-catenin targets, expression of adipose lineage or fibroblastic markers were not significantly altered (Figure S3C).

To test if β-catenin activation altered adipose progenitor lineage decisions, we labeled the progenitors by crossing a TRE-H2B-GFP (H2B = Histone 2B) reporter into P-BCA mice. In this system, H2B-GFP is stably incorporated into the chromatin of adipose lineage cells (Tang et al., 2011; Tang et al., 2008; Zeve et al., 2009). If cells within the lineage continue to express PPARγ, GFP is expressed. However, if the number of progenitors is reduced or if PPARγ expression is blunted, for example secondary to fate changes, GFP expression is reduced (Figure 3F) (Tang et al., 2011; Tang et al., 2008; Zeve et al., 2009). We found that P-BCA IGW had much less GFP fluorescence, and presumably reduced PPARγ expression or adipose lineage formation, but that PGW depots had normal fluorescence (Figure 3G). Flow cytometric analyses showed that P-BCA SQ depots had fewer progenitors (Figure 3H).

To test the possibility that Wnt activation changed the fate of adipose progenitors into a fibroblastic lineage, we crossed a rosa26-flox-stop-flox-LacZ (R26R) allele into P-BCA mice (Soriano, 1999; Tang et al., 2008) thereby indelibly marking adipose progenitor cells and all descendants (Figure 3I) (Tang et al., 2011; Tang et al., 2008; Zeve et al., 2009). Notably, the cells present within the fibrotic tissues expressed lacZ, and therefore derived from a PPARγ-positive cell, and contained high levels of nuclear β-catenin (Figures 3J, 3K and S3D). Thus, the cells present within the fibrotic depots express fibroblastic markers, descend from the adipose lineage, and have an activated Wnt pathway.

To further investigate a possible adipose progenitor fate change, we isolated SQ SVF from control and P-BCA mice, cultured the cells in adipogenic conditions, and then stained them with Oil Red O as an indicator of adipogenesis. P-BCA mutant SVF failed to differentiate

(Figure 3L). qPCR analyses after induction confirmed the adipogenic blockade and showed high levels of Wnt targets, as well as preadipocyte (e.g., Pref-1) and fibroblastic markers (Figure 3M). PPARγ regulates the adipogenic fate, and thus, to determine if the cells retained adipogenic potential, we infected control and P-BCA SQ SVF cells with a virus expressing PPARγ. However, PPARγ infection of P-BCA cells failed to rescue the adipogenic phenotype (Figure 3N and 3O).

P-BCA Mutants Do Not Develop Classical Metabolic Consequences of Lipodystrophy

Lipodystrophy, the pathological reduction in fat content, is accompanied by multiple metabolic disturbances, notably hyperlipidemia and secondary ectopic lipid deposition (e.g., fatty liver), insulin resistance and hyperglycemia (Fiorenza et al., 2010; Garg, 2004). Based upon MRI and NMR analyses, as well as the paucity of circulating adipokines such as adiponectin and leptin (Figure 2D-2H), we reasoned that P-BCA mice were likely to have lipodystrophic metabolic disturbances. Consistent with that notion, the blood triglyceride (TG) levels of P-BCA mutants were elevated at comparable levels to PPARγ null mice, a lipodystrophic model (Figure 4A). Surprisingly, however, liver histology and triglyceride quantitation showed that P-BCA mutants did not deposit fat in the liver, which, in lipodystrophic and hyperlipidemic models, is a typical storage site for excess triglycerides, as seen in PPARγ null livers (Figure 4B) (Fiorenza et al., 2010; Garg, 2004). This unexpected absence of a hallmark lipodystrophic consequence raised the possibility that glucose and insulin homeostasis also might not show the typical lipodystrophic hyperglycemia and hyperinsulinemia. Indeed, fed blood glucose and insulin levels were similar between controls and mutants and quite different from PPARγ null lipodystrophic mice (Figure 4C).

Next, we quantified food intake, movement, oxygen consumption and respiratory quotient (RQ). The P-BCA mice displayed a modest increase in activity and food intake during the light cycle when mice sleep (Figure 4D and 4E); however, oxygen consumption was not statistically altered (Figure S4A). Further, the RQ values indicated that carbohydrates, rather than fatty acids, were preferentially utilized during that time (Figure S4B), consistent with the increased food intake.

To investigate whether the increased RQ, activity, and food consumption was due to fasting-induced hypoglycemia, we quantified blood glucose at baseline and one hour after food removal. Although initial fed glucose levels were equal, P-BCA mutants, but not controls, lowered their blood glucose within one hour of food withdrawal (Figure 4F). Glucose tolerance tests (GTTs) also showed that P-BCA glucose levels were low, opposite of classical lipodystrophy (e.g., PPARγ null) (Figure 4G and 4H). High insulin levels could explain the hypoglycemia. However, fasting decreased serum insulin levels in parallel with reduced blood glucose (Figure 4I). We quantified fasted serum levels of other glucose regulatory molecules, including IGF-1, IGF-2, glucagon and growth hormone, but found no change compared to controls, with IGF-2 undetectable in both control and mutant sera (Figure 4J, not shown).

P-BCA Mutant Mice Have Normal Insulin Sensitivity and Do Not Require Insulin for Reduced Blood Glucose

Increased sensitivity to insulin, rather than levels, could cause fasting hypoglycemia. However, exogenous insulin reduced glucose levels to the same extent in controls and mutants (Figure 5A). Next, we probed Akt phosphorylation, an indicator of insulin signaling, before and 15 minutes after insulin injection. Western blots of muscle extracts showed that insulin increased the level of Akt phosphorylation, and that Akt phosphorylation was not altered by the P-BCA mutation (Figure 5B). These data indicate

that the insulin responsiveness of P-BCA mutants was unchanged and might not cause the observed hypoglycemia.

To investigate whether insulin action was required for the paradoxical P-BCA hypoglycemia, we blocked insulin secretion through two methods. In one, we infused somatostatin, a hormone that inhibits secretion of insulin and glucagon (Sakurai et al., 1974), and examined glucose levels during fasting and in GTTs (Figure 5C). We used a dose of somatostatin that eliminated insulin secretion in fasted mutants, but just decreased insulin levels in controls, exploiting the lower fasting insulin levels of the mutants (Figures 4I and 5D). Thus mutants would not have the glucose-lowering effect of insulin, while controls would. Nonetheless, food withdrawal still reduced P-BCA glucose levels and P-BCA mice had a muted response and a rapid return to baseline in GTTs (Figure 5C). We also administered streptozotocin (STZ), a small molecule that destroys insulin-producing pancreatic beta cells (Pieper et al., 1999), to control and P-BCA siblings. Consistent with beta cell destruction, blood glucose levels increased and insulin became almost undetectable (Figure 5E and 5F). Nonetheless, P-BCA mice given STZ maintained a significantly lower blood sugar level in GTTs compared to STZ controls (Figure 5E). These data indicate that at least part of the observed hypoglycemia and increased glucose tolerance is independent of insulin signaling.

Muscles of P-BCA Mutants Have Increased Glucose Uptake, Increased AMPK and Glucose Transporter Activity, but Unaltered Wnt Signaling

In a “fed GTT”, in which control and mutant siblings were challenged with a glucose load without prior fasting, P-BCA mutants cleared glucose more efficiently than controls (Figure 6A). Next we performed hyperinsulinemic euglycemic clamps in which a constant amount of insulin is infused to increase and equalize sera insulin along with a variable amount of glucose to maintain blood glucose levels at a constant level of approximately 130 mg/dL (Figure 6B and S5). Once the glucose levels were equalized, the glucose infusion rate (GIR) was five times higher in mutants compared to controls (Figure 6C), indicating that P-BCA mutants remove glucose from the blood at much higher rates at equal sera concentrations of insulin. To examine which tissues might have increased glucose uptake, we injected low levels of ^{14}C-labeled and metabolically-inert 2-deoxy glucose at the end of clamps and found that P-BCA skeletal and cardiac muscles absorbed between 2–4 times more glucose than control (Figure 6D).

Skeletal muscle can increase glucose uptake through insulin dependent and independent mechanisms (Steinberg and Kemp, 2009). AMPK activation is a key mediator of the latter, enhancing muscle glucose utilization during exercise (Fujii et al., 2006). Since the glucose lowering effect observed in P-BCA mice can occur in an insulin-independent manner (Figure 5), we examined the levels of AMPK activity, using Western blots for AMPK and acetyl-CoA carboxylase (ACC, an AMPK target) phosphorylation, in control and mutant muscles (Steinberg and Kemp, 2009). We found increased AMPK and ACC phosphorylation in mutant muscles compared to controls in both the fed and fasted milieu (Figure 6E). We also analyzed p38 mitogen-activated protein kinase (MAPK), as it has been shown to be involved in muscle glucose uptake (Chambers et al., 2009; Lemieux et al., 2003; Somwar et al., 2000). Compared to controls, P-BCA mutants have increased activation of p38 MAPK, as measured by phosphorylation, without increased insulin signaling, as measured by Akt phosphorylation (Figure 6E). To examine AMPK necessity, we injected P-BCA mutants with vehicle or Compound C, an AMPK inhibitor (Zhou et al., 2001). Compound C reduced AMPK phosphorylation, rescued fasting-induced hypoglycemia, and induced fasting hyperglycemia, which was exaggerated by GTT (Figure 6F-6H).

In muscle, AMPK and p38 MAPK increase glucose uptake by stimulating the translocation of glucose transporters to the cell surface (Lemieux et al., 2003; Steinberg and Kemp, 2009). To explore such a potential mechanism we analyzed membrane fractions of control and mutant muscles, from mice with or without STZ treatment, for levels of glucose transporters. We found that plasma membranes of P-BCA muscle had higher levels of Glut4, and to a lesser extent Glut1, than controls (Figures 6I), even in the absence of insulin.

We next addressed the possibility that the functional changes observed in muscle were due to tissue autonomous actions, which could occur if the Cre driver was expressed in the myogenic lineage. We first lineage traced the Cre driver using the indelible Rosa26 marking system to assess the integrated history of the driver in muscles during development and adulthood. However, we did not detect significant muscle X-gal staining (Figure 6J). Further, the faster-migrating activated form of β-catenin observed in adipose tissue was not detected in muscle extracts (Figure 6K). We also examined Wnt target genes expression. However, qPCR analyses did not support the idea that the Wnt pathway was activated in mutant muscle (Figure 6L). These data indicate that Wnt activation at distance sites alters muscle to increase glucose uptake in a non-autonomous manner. Mechanistically, this may occur via AMPK, and p38 MAPK, activation and increased glucose transporter cell surface localization.

P-BCA Sera and P-BCA SV Cell Conditioned Media Increase Glucose Uptake in Wild-Type Muscle Explants

To further discriminate between intrinsic and extrinsic differences in P-BCA muscles, we turned to an *ex vivo* glucose uptake assay. We explanted sibling control and P-BCA tibialis anterior (TA) and extensor digitorum longus (EDL) muscles, and at time zero assayed glucose uptake using radio-labeled 2-deoxyglucose. We found that P-BCA muscles had increased glucose uptake, mirroring the euglycemic clamps (Figure 6D, 7A, not shown). We then assayed glucose uptake after control and P-BCA muscles were incubated in wild-type (C57BL/6) sera for three hours. This pre-incubation equalized glucose uptake indicating that the *in vivo* changes might be secondary to extrinsic factors (Figure 7A).

To test that notion, we isolated TA and EDL muscles from wild-type C57BL/6 mice and incubated the explants in sibling control sera and P-BCA sera, for either one or three hours, and then assayed glucose uptake. We also included wild-type sera without or with supraphysiological insulin (~1000x fed sera concentration), as a positive control. At both times, PBCA sera stimulated glucose uptake significantly more than control sera, similar to exogenous insulin (Figure 7B and 7C). We also evaluated the wild-type muscle explants for signaling 15 minutes after incubation in these conditions. We found that insulin increased Akt, but not AMPK, phosphorylation (Figure 7D). In contrast, P-BCA sera appeared to activate AMPK, but not Akt (Figure 7E).

To investigate the possibility that SQ adipose progenitors, those cells that had undergone a lineage change, produced the activity, we generated and cultured SV cells from SQ depots of control and P-BCA littermates, and collected conditioned media. We incubated wild-type muscle explants in the conditioned media and then assessed glucose uptake. The conditioned media from the P-BCA mutant cells increased glucose uptake significantly more than control conditioned media (Figure 7F). Together, these studies indicate that the P-BCA mutant sera and the P-BCA mutant SVF secretome contains a factor(s) that acts upon muscles to activate AMPK and augment glucose uptake, potentially accounting for aspects of the observed *in vivo* P-BCA metabolic phenotypes (Figure 7G).

DISCUSSION

Metabolism and glucose homeostasis are regulated by interactions, often mediated via non-autonomous signals, of many tissues. Due to the inherent systemic dependencies, elucidation of physiology and endocrine regulation often stems from *in vivo* modeling. For example, the breakthrough discovery of leptin and the role of adipose tissue as a key site of hormone production and secretion relied upon mouse models followed over decades by physiological and molecular understanding (Friedman, 2010).

To investigate underpinnings of metabolic biology, we utilized genetic modeling. When canonical Wnt signaling was altered within mammalian adipose progenitor cells and throughout the lineage, several distinct phenotypes were produced. For example, there appeared to be adipose depot specificity. Although the fat content of both subcutaneous and visceral depots was severely diminished, the manner in which this occurred was qualitatively distinct. The mutant visceral depots were significantly smaller than controls, while subcutaneous adipose tissues were normal size. The disparity between the lack of triglyceride accumulation and the absence of adipocytes, yet characteristic SQ depot morphology, is reconciled by replacement of the adipocyte lineage by fibroblastic cells. Notably these fibroblastic lineage cells derived from the adipose progenitor compartment, indicating that SQ progenitor fate is regulated by Wnt signals.

aP2-dependent β-catenin activation (A-BCA) within mature adipocytes did not produce discernable metabolic effects while a PPARγ driver (P-BCA) in adipose progenitor cells produced striking metabolic phenotypes. Perhaps the most surprising results of altering Wnt signaling within the adipose progenitor compartment were the anomalous constellation of phenotypes that seem paradoxical to reports on classical lipodystrophy (Longo et al., 2004; Savage, 2009; Wright et al., 2007). Although P-BCA mice lacked adipose triglyceride accumulation, with hypertriglyceridemia that mirrored classical lipodystrophies, ectopic fatty acid accumulation and hyperglycemia were notably absent. Rather, the mice appeared protected from toxic fatty deposition and were hypoglycemic.

Since understanding glucose homeostasis has important ramifications, we explored both the physiological and the molecular underpinnings of the seemingly idiosyncratic P-BCA glucose levels using a series of static, dynamic and provocative tests. Increased muscle glucose uptake appeared to be an important catalyst of the improved glucose homeostasis. This enhanced glucose absorption can occur independently of insulin action. The physiological studies pointed to a testable mechanistic hypothesis: were AMPK and p38 MAPK, both of which can increase glucose uptake in muscle independently of insulin action, activated in P-BCA muscles. Biochemical studies supported this notion, as the mutant muscles had increased AMPK and p38 MAPK activity, along with increased plasma membrane localization of glucose transporters.

Since the implications of a possible non-autonomous signal altering muscle function are significant, we examined the possibility that the Wnt pathway was altered within the myogenic lineage *per se* through a variety of studies. However, lineage tracing and molecular analyses did not support that idea. To further investigate possible extrinsic signals, we established an organotypic culture system for measuring intact muscle glucose uptake. With this *ex vivo* system we found that the increase in glucose uptake in the mutant muscles was present immediately after placing the explants in culture, mirroring the euglycemic clamp, but thereafter was reversible. That is, the increase in glucose uptake did not appear intrinsic to the muscles, pointing to the presence of a possible hormonal factor. Indeed, cultures of wild-type muscle incubated in mutant sera had significant increases in glucose uptake and AMPK activation, but not Akt activation, compared to control sera.

Previous studies have illuminated an active communication network between adipose tissue and muscle to regulate glucose homeostasis. The adipokines adiponectin and leptin can increase muscle insulin sensitivity and glucose uptake, through indirect and direct means (Tomas et al., 2002; Toyoshima et al., 2005). However, the levels of these two hormones were markedly diminished or undetectable in P-BCA mutant sera, supporting the possibility that other such factors may derive from the mutant adipose depots, from adipose lineage cells residing in other locations, and/or from non-adipose lineage. The importance of testing such a notion is further highlighted by the possibility that the PPARγ-tTA, TRE-Cre driver may be expressed in non-adipose tissues either non-specifically or specifically; PPARγ is expressed in a variety of cell types (Michalik et al., 2002). That is the use of the PPARγ promoter/enhancer elements confounds phenotypic interpretation, especially cells of origin of the postulated glucose dynamics factor and whether the signal derives from adipose lineage cells. Another potential complication is that adipose stem cells might reside in non-adipose depot locales. Notable among these are reports that adipose progenitors are present within skeletal muscle, and that these cells can regulate muscle function (Joe et al., 2010; Uezumi et al., 2010). Thus it is possible that muscle-resident adipose progenitors could alter muscle glucose metabolism via an intramuscular means. We attempted to probe the possibility that the altered skeletal muscle glucose uptake might be secondary to intrinsic effects with several methods including lineage studies as well as with analyses of beta-catenin recombination and Wnt target gene activation. Although these studies were negative, they are limited by detection sensitivity and other factors. *Ex vivo* organotypic muscle glucose uptake assays indicated that the increased muscle glucose uptake might not be intrinsic as the effect was present immediately but thereafter was reversible. *Ex vivo* muscle studies also showed that mutant sera could recapitulate *in vivo* hallmarks of the P-BCA mice: increased glucose uptake and activation of AMPK. Nonetheless, these studies do not exclude potential intramuscular effects. Further, the secretion of the postulated glucose dynamics factor may not derive from the mutant adipose tissue or β-catenin activation *per se*, as secondary changes in peripheral tissues (e.g., liver, brain) could be responsible. Notably, conditioned media from P-BCA SV cells, in which adipose progenitors reside, stimulated glucose uptake significantly more than control SV conditioned media. Further approaches, such as analyses of mutant adipose stem cells, stem cell transplants, identification and expression analyses of candidate factors and further mechanistic dissection will be required to define the signal, to determine its origin, and to delineate how it functions. Taken together, our studies indicate that blood glucose levels can be reduced via a non-autonomous signal, possibly from Wnt-activated subcutaneous progenitors or their derivatives or other adipose stroma-resident cells, that increases AMPK activity and glucose uptake in muscle (Figure 7G) and provide a platform for discovery of the potential glucose-regulatory factor.

Materials and Methods

Mouse Studies

The aP2-Cre, PPARγ-tTA, TRE-Cre, fBC, TRE-H2B-GFP and R26R mice were maintained as described and used to generate controls, A-BCA, P-BCA and lineage reporter mouse lines (Tang et al., 2011; Tang et al., 2008). Mice were fed normal chow (4% fat, Teklad). Fat content was measured using a minispec mq10 NMR Analyzer (Bruker). For GTTs and ITTs, 1.25mg glucose or 1.5mU Humalog (Lilly)/1g mouse weight was injected intraperitoneally (IP) after a 5 hour fast (for GTT) or during normal feeding (for fed GTT and ITT), blood glucose levels were measured at the indicated intervals (Seo et al., 2009). To induce a diabetic phenotype 0.2mg STZ /1g mouse was injected IP (Pieper et al., 1999). To block AMPK activation 30mg Compound C/kg mouse was injected IP (Kim et al., 2004). Veterinary care provided by Division of Comparative Medicine. Animals maintained under

UT Southwestern Medical Center Animal Care and Use Committee guidelines according to current NIH guidelines.

Metabolic Phenotyping Experiments

Clamp studies were performed at the UT Southwestern Medical Center Metabolic Core at Dallas based on previously described methods (Berglund et al., 2008). In brief, mice were anesthetized (Oxygen flow rate: 0.5–1 liter/min and isoflurane concentration: 2–3%) and the jugular vein was catheterized. Mice were monitored for 5 days and mice that remained within 10% of the pre-surgical body weight were studied. The clamp was started at t = 0 min with a continuous insulin infusion (2.5mU/kg/min) 5 hours after fasting. Glucose was measured every 10 minutes for 2 hours to maintain euglycemia (130mg/dL) using a variable glucose infusion rate (GIR). 2-[1-^{14}C]-deoxy-D-glucose was administered at 120 minutes to measure tissue-specific glucose uptake. Tissues were collected to determine glucose uptake, normalized to brain uptake. For somatostatin experiments, catheterized mice were fasted for 2 hours and somatostatin (3 ug/kg/min) was infused at 0 minutes to prevent pancreatic secretion of insulin and glucagon. A GTT was performed at 120 minutes.

Histology

Tissues were formalin-fixed and paraffin-embedded. 5–8 micron sections were cut and stained with hematoxylin and eosin or trichrome. For immunostaining, sections were deparaffinized, boiled in antigen-retrieval solution, treated with β-catenin or Fsp-1 antibody, stained with Vectastain ABC KIT (Vector Laboratories) and DAB (Thermo Scientific).

qPCR

Total RNA was extracted using TRIzol (Invitrogen), DNaseI-treated, reverse-transcribed with random hexamers, gene expression was analyzed using ABI 7500 Real-Time PCR System (Seo et al., 2009) and values normalized by beta-actin expression. Primer sequences available upon request.

Westerns

Immunoblotting was performed according to standard procedures (Seo et al., 2005). Protein was extracted using PhosphoSafe Extraction Reagent (Calbiochem), boiled, separated on denaturing polyacrylamide gels, and transferred. Membranes were blocked and incubated with primary antibodies [total and phospho (Thr 172) AMPK, total and phospho (Ser 79) ACC, total and phospho (Thr 180/ Tyr 182) p38 MAPK, total and phospho (Ser 473) Akt, insulin receptor (IR), cadherin, β-catenin, Glut4, and tubulin from Cell Signaling Technology; Fsp-1 and Glut1 from Abcam], washed and incubated with secondary antibodies conjugated with HRP (Jackson ImmunoResearch). Signals were detected with chemiluminescent kits (NEN).

Cell Fractionation

Fractionation was performed as previously described with slight modification (Carvalho et al., 2004). Muscle tissue from hind legs of control and P-BCA mice were removed, frozen, powdered, suspended in HB buffer (20mM Tris, 1mM EDTA, 255mM Sucrose, pH 7.4), and homogenized. The supernatant was centrifuged at 16,000g for 20 minutes after tissue debris was removed. The pellet was resuspended with HB buffer and centrifuged on 1.12M sucrose cushion at 100,000g for 15 minutes. Plasma membrane fraction was collected from the interface, diluted with HB buffer and centrifuged at 200,000g for 15 minutes. The pellet was resuspended in SDS lysis buffer, sonicated, centrifuged, and the supernatant was used as plasma membrane fraction.

Isolation of Adipose Progenitor Cells

Floating adipocytes and SV cells were isolated as described (Tang et al., 2008).

Cell Culture

SV cells were cultured in DMEM with 10% FBS, 100units/ml penicillin and 100μg/ml streptomycin. For induction, confluent wells were maintained in growth media supplemented with 1μg/ml insulin for about one week. Oil Red O staining was performed as described (McKay et al., 2003). Recombinant retroviral production and transduction was performed as described (Suh et al., 2006). For conditioned media, the SV cells were cultured to confluence and the media was collected every 24 hours. In each conditioned media study, the SV cells were from at least three control and three mutant siblings.

Ex Vivo Muscle Glucose Uptake

Intact TA and EDL muscles from: C57BL/6, sibling controls or P-BCA mutants were dissected. For glucose uptake assays, the muscles were incubated in the indicated conditions, rinsed, placed into 100 ul of glucose-free DMEM containing 2-deoxy-glucose and ^{3}H-2-deoxy-glucose for 20 minutes, rinsed in ice-cold PBS, and radioactive incorporation assessed in scintillation fluid and normalized to muscle weight. In the various sera incubations, the left or right muscle of the same mouse was placed into either control or the test condition, these include: wild-type C57BL/6 sera or B6 sera containing 0.1U insulin (Humalog, ~40,000ng/ml), as well as sibling control or PBCA mutant sera. In each study, muscles were obtained from at least 4 mice per group and sera were from at least 3 different mice.

X-gal Staining

X-gal staining was performed as described (Tang et al., 2008).

Statistical Analysis

Statistical significance assessed by two-tailed Student's t-test. Error bars indicate SEM.

Research Highlights

- β-catenin activation in fat progenitors induces a fibroblastic cell fate change
- Lipodystrophic PBCA mice lack fat but have improved glucose homeostasis
- Glucose uptake is increased in muscles of PBCA mice in an insulin-independent manner
- Adipose progenitors secrete a glucose regulatory factor in response to Wnt activation

Supplementary Material

Refer to Web version on PubMed Central for supplementary material.

Acknowledgments

We thank Drs. Joseph Avruch, Perry Blackshear, Michael Brown, Joseph Goldstein, Makoto Taketo, Michelle Tallquist, Joel Elmquist and Luis Parada for generously providing reagents, instruments and thoughtful discussion, Shawna Kennedy and Ashley Stephenson for their excellent technical support and members of the Graff Lab for invaluable insights and suggestions. We thank the UT Southwestern Mouse Metabolic Phenotyping Core (MMPC) and Kenneth Coulter from UTSW Biomedical Communications. Mouse sera hormone tests were done by the Cincinnati MMPC, supported in part by grant U24 DK059630. This study supported by NIH and NIDDK grants

(R01 DK066556, R01 DK064261 and R01 DK088220), postdoctoral fellowship grants (J.S. and W.T.) and predoctoral fellowship grant (D.Z.) from the AHA South Central Affiliate. J.M.G. is a founder of Reata Pharmaceuticals.

REFERENCES

Bennett CN, Ross SE, Longo KA, Bajnok L, Hemati N, Johnson KW, Harrison SD, MacDougald OA. Regulation of Wnt signaling during adipogenesis. J Biol Chem. 2002; 277:30998–31004. [PubMed: 12055200]

Berglund ED, Li CY, Poffenberger G, Ayala JE, Fueger PT, Willis SE, Jewell MM, Powers AC, Wasserman DH. Glucose metabolism in vivo in four commonly used inbred mouse strains. Diabetes. 2008; 57:1790–1799. [PubMed: 18398139]

Carvalho E, Schellhorn SE, Zabolotny JM, Martin S, Tozzo E, Peroni OD, Houseknecht KL, Mundt A, James DE, Kahn BB. GLUT4 overexpression or deficiency in adipocytes of transgenic mice alters the composition of GLUT4 vesicles and the subcellular localization of GLUT4 and insulin-responsive aminopeptidase. J Biol Chem. 2004; 279:21598–21605. [PubMed: 14985357]

Chambers MA, Moylan JS, Smith JD, Goodyear LJ, Reid MB. Stretch-stimulated glucose uptake in skeletal muscle is mediated by reactive oxygen species and p38 MAP-kinase. J Physiol. 2009; 587:3363–3373. [PubMed: 19403598]

DeFronzo RA, Tripathy D. Skeletal muscle insulin resistance is the primary defect in type 2 diabetes. Diabetes Care. 2009; 32 Suppl 2:S157–S163. [PubMed: 19875544]

Duan SZ, Ivashchenko CY, Whitesall SE, D'Alecy LG, Duquaine DC, Brosius FC 3rd, Gonzalez FJ, Vinson C, Pierre MA, Milstone DS, et al. Hypotension, lipodystrophy, and insulin resistance in generalized PPARgamma-deficient mice rescued from embryonic lethality. J Clin Invest. 2007; 117:812–822. [PubMed: 17304352]

El-Bizri N, Wang L, Merklinger SL, Guignabert C, Desai T, Urashima T, Sheikh AY, Knutsen RH, Mecham RP, Mishina Y, et al. Smooth muscle protein 22alpha-mediated patchy deletion of Bmpr1a impairs cardiac contractility but protects against pulmonary vascular remodeling. Circ Res. 2008; 102:380–388. [PubMed: 18079409]

Fiorenza CG, Chou SH, Mantzoros CS. Lipodystrophy: pathophysiology and advances in treatment. Nat Rev Endocrinol. 2010

Friedman JM. A tale of two hormones. Nat Med. 2010; 16:1100–1106. [PubMed: 20930753]

Fujii N, Jessen N, Goodyear LJ. AMP-activated protein kinase and the regulation of glucose transport. Am J Physiol Endocrinol Metab. 2006; 291:E867–E877. [PubMed: 16822958]

Galic S, Oakhill JS, Steinberg GR. Adipose tissue as an endocrine organ. Mol Cell Endocrinol. 2010; 316:129–139. [PubMed: 19723556]

Garg A. Acquired and inherited lipodystrophies. N Engl J Med. 2004; 350:1220–1234. [PubMed: 15028826]

Garvey WT, Maianu L, Zhu JH, Brechtel-Hook G, Wallace P, Baron AD. Evidence for defects in the trafficking and translocation of GLUT4 glucose transporters in skeletal muscle as a cause of human insulin resistance. J Clin Invest. 1998; 101:2377–2386. [PubMed: 9616209]

Hayashi S, Lewis P, Pevny L, McMahon AP. Efficient gene modulation in mouse epiblast using a Sox2Cre transgenic mouse strain. Gene Expr Patterns. 2002; 2:93–97. [PubMed: 12617844]

Huang S, Czech MP. The GLUT4 glucose transporter. Cell Metab. 2007; 5:237–252. [PubMed: 17403369]

Joe AW, Yi L, Natarajan A, Le Grand F, So L, Wang J, Rudnicki MA, Rossi FM. Muscle injury activates resident fibro/adipogenic progenitors that facilitate myogenesis. Nat Cell Biol. 2010; 12:153–163. [PubMed: 20081841]

Kahn BB, Alquier T, Carling D, Hardie DG. AMP-activated protein kinase: ancient energy gauge provides clues to modern understanding of metabolism. Cell Metab. 2005; 1:15–25. [PubMed: 16054041]

Kim EK, Miller I, Aja S, Landree LE, Pinn M, McFadden J, Kuhajda FP, Moran TH, Ronnett GV. C75, a fatty acid synthase inhibitor, reduces food intake via hypothalamic AMP-activated protein kinase. J Biol Chem. 2004; 279:19970–19976. [PubMed: 15028725]

Lemieux K, Konrad D, Klip A, Marette A. The AMP-activated protein kinase activator AICAR does not induce GLUT4 translocation to transverse tubules but stimulates glucose uptake and p38 mitogen-activated protein kinases alpha and beta in skeletal muscle. FASEB J. 2003; 17:1658–1665. [PubMed: 12958172]

Longo KA, Wright WS, Kang S, Gerin I, Chiang SH, Lucas PC, Opp MR, MacDougald OA. Wnt10b inhibits development of white and brown adipose tissues. J Biol Chem. 2004; 279:35503–35509. [PubMed: 15190075]

McKay RM, McKay JP, Avery L, Graff JM. C elegans: a model for exploring the genetics of fat storage. Dev Cell. 2003; 4:131–142. [PubMed: 12530969]

Michalik L, Desvergne B, Dreyer C, Gavillet M, Laurini RN, Wahli W. PPAR expression and function during vertebrate development. Int J Dev Biol. 2002; 46:105–114. [PubMed: 11902671]

Morton GJ, Cummings DE, Baskin DG, Barsh GS, Schwartz MW. Central nervous system control of food intake and body weight. Nature. 2006; 443:289–295. [PubMed: 16988703]

Must A, Spadano J, Coakley EH, Field AE, Colditz G, Dietz WH. The disease burden associated with overweight and obesity. JAMA. 1999; 282:1523–1529. [PubMed: 10546691]

Pieper AA, Brat DJ, Krug DK, Watkins CC, Gupta A, Blackshaw S, Verma A, Wang ZQ, Snyder SH. Poly(ADP-ribose) polymerase-deficient mice are protected from streptozotocin-induced diabetes. Proc Natl Acad Sci U S A. 1999; 96:3059–3064. [PubMed: 10077636]

Rodeheffer MS, Birsoy K, Friedman JM. Identification of white adipocyte progenitor cells in vivo. Cell. 2008; 135:240–249. [PubMed: 18835024]

Ross SE, Hemati N, Longo KA, Bennett CN, Lucas PC, Erickson RL, MacDougald OA. Inhibition of adipogenesis by Wnt signaling. Science. 2000; 289:950–953. [PubMed: 10937998]

Sakahara M, Ohkawara H, Nakao K, Yokozaki H, Aiba A. The simultaneous induction of tumorigenesis and Cre-loxP recombination in mice. Kobe J Med Sci. 2009; 54:E279–E289. [PubMed: 19628969]

Sakurai H, Dobbs R, Unger RH. Somatostatin-induced changes in insulin and glucagon secretion in normal and diabetic dogs. J Clin Invest. 1974; 54:1395–1402. [PubMed: 4436439]

Savage DB. Mouse models of inherited lipodystrophy. Dis Model Mech. 2009; 2:554–562. [PubMed: 19892886]

Seo J, Fortuno ES >3rd, Suh JM, Stenesen D, Tang W, Parks EJ, Adams CM, Townes T, Graff JM. Atf4 regulates obesity, glucose homeostasis, and energy expenditure. Diabetes. 2009; 58:2565–2573. [PubMed: 19690063]

Seo J, Lozano MM, Dudley JP. Nuclear matrix binding regulates SATB1-mediated transcriptional repression. J Biol Chem. 2005; 280:24600–24609. [PubMed: 15851481]

Somwar R, Perreault M, Kapur S, Taha C, Sweeney G, Ramlal T, Kim DY, Keen J, Cote CH, Klip A, et al. Activation of p38 mitogen-activated protein kinase alpha and beta by insulin and contraction in rat skeletal muscle: potential role in the stimulation of glucose transport. Diabetes. 2000; 49:1794–1800. [PubMed: 11078445]

Soriano P. Generalized lacZ expression with the ROSA26 Cre reporter strain. Nat Genet. 1999; 21:70–71. [PubMed: 9916792]

Steinberg GR, Kemp BE. AMPK in Health and Disease. Physiol Rev. 2009; 89:1025–1078. [PubMed: 19584320]

Strilic B, Kucera T, Lammert E. Formation of cardiovascular tubes in invertebrates and vertebrates. Cell Mol Life Sci. 2010; 67:3209–3218. [PubMed: 20490602]

Suh JM, Gao X, McKay J, McKay R, Salo Z, Graff JM. Hedgehog signaling plays a conserved role in inhibiting fat formation. Cell Metab. 2006; 3:25–34. [PubMed: 16399502]

Tang W, Zeve D, Seo J, Jo AY, Graff JM. Thiazolidinediones regulate adipose lineage dynamics. Cell Metab. 2011; 14:116–122. [PubMed: 21723509]

Tang W, Zeve D, Suh JM, Bosnakovski D, Kyba M, Hammer RE, Tallquist MD, Graff JM. White fat progenitor cells reside in the adipose vasculature. Science. 2008; 322:583–586. [PubMed: 18801968]

Tomas E, Tsao TS, Saha AK, Murrey HE, Zhang Cc, C, Itani SI, Lodish HF, Ruderman NB. Enhanced muscle fat oxidation and glucose transport by ACRP30 globular domain: acetyl-CoA carboxylase

inhibition and AMP-activated protein kinase activation. Proc Natl Acad Sci U S A. 2002; 99:16309–16313. [PubMed: 12456889]

Toyoshima Y, Gavrilova O, Yakar S, Jou W, Pack S, Asghar Z, Wheeler MB, LeRoith D. Leptin improves insulin resistance and hyperglycemia in a mouse model of type 2 diabetes. Endocrinology. 2005; 146:4024–4035. [PubMed: 15947005]

Uezumi A, Fukada S, Yamamoto N, Takeda S, Tsuchida K. Mesenchymal progenitors distinct from satellite cells contribute to ectopic fat cell formation in skeletal muscle. Nat Cell Biol. 2010; 12:143–152. [PubMed: 20081842]

Wright WS, Longo KA, Dolinsky VW, Gerin I, Kang S, Bennett CN, Chiang SH, Prestwich TC, Gress C, Burant CF, et al. Wnt10b inhibits obesity in ob/ob and agouti mice. Diabetes. 2007; 56:295–303. [PubMed: 17259372]

Zeve D, Tang W, Graff J. Fighting fat with fat: the expanding field of adipose stem cells. Cell Stem Cell. 2009; 5:472–481. [PubMed: 19896439]

Zhou G, Myers R, Li Y, Chen Y, Shen X, Fenyk-Melody J, Wu M, Ventre J, Doebber T, Fujii N, et al. Role of AMP-activated protein kinase in mechanism of metformin action. J Clin Invest. 2001; 108:1167–1174. [PubMed: 11602624]

Zierath JR, He L, Guma A, Odegoard Wahlstrom E, Klip A, Wallberg-Henriksson H. Insulin action on glucose transport and plasma membrane GLUT4 content in skeletal muscle from patients with NIDDM. Diabetologia. 1996; 39:1180–1189. [PubMed: 8897005]

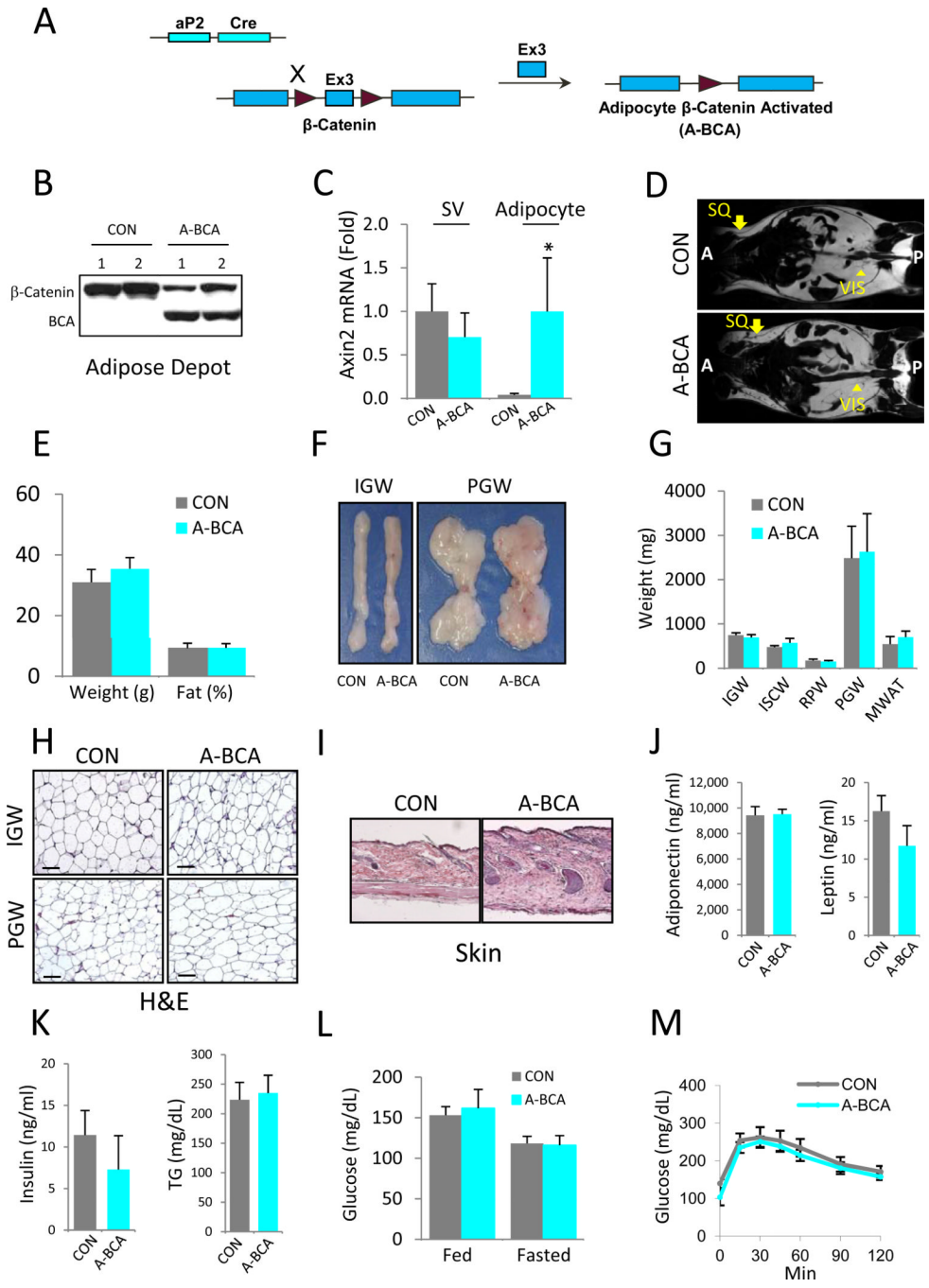

Figure 1. β-Catenin Activation in Mature Adipocytes Does Not Alter Adiposity or Glucose Homeostasis

(A) Schematic of mature adipocyte cell-autonomous activation of β-catenin using aP2-Cre. Maroon arrowheads represent LoxP sites.

(B) Western blot of control (CON) and A-BCA mutant inguinal adipose depot extracts using an anti-β-catenin antibody. Slower migrating bands represent wild-type form (β-Catenin); faster migrating bands represent the activated form of β-catenin (BCA).

(C) qPCR analysis of Wnt target gene Axin2 in the stromal vascular fraction (SV) and adipocyte fraction of control and A-BCA mice.

(D) Magnetic Resonance Images of control and A-BCA mice. Arrows indicate subcutaneous (SQ) adipose depots; arrowheads indicate visceral (VIS) adipose depots. Anterior (A); Posterior (P).
(E) Weight and percent body fat (from NMR spectroscopy) of control and A-BCA siblings.
(F) Explants of inguinal (IGW) and perigonadal (PGW) adipose depots of control and A-BCA siblings.
(G) Weights of the indicated adipose depots of control and A-BCA mice. IGW = inguinal white adipose tissue (WAT), ISCW = intrascapular WAT, RPW = retroperitoneal WAT, PGW = perigonadal WAT, MWAT = mesenteric WAT.
(H) Histological sections of control and A-BCA mutant inguinal (IGW) and perigonadal (PGW) depots stained with hematoxylin and eosin (H&E). Size bar = 100μm.
(I) Histological sections of control and A-BCA skin stained with H&E.
(J, K) Control and A-BCA serum levels of adiponectin and leptin (J) and insulin and triglyceride (TG) (K).
(L) Blood glucose levels of fed or fasted (4 hours) control and A-BCA siblings.
(M) Glucose tolerance tests after a 4-hour fast of control and A-BCA siblings.
Representative studies on 4-month old sibling males; $n \geq 8$ per cohort, repeated ≥ 3 cohorts. Female data also showed no effect elicited by the A-BCA mutation. Error bars indicate SEM. Statistical significance assessed by two-tailed Student's t-test, $*p<0.05$. Genotypes: Control = roughly equal mixture of aP2-Cre or fBC. A-BCA = aP2-Cre; fBC.

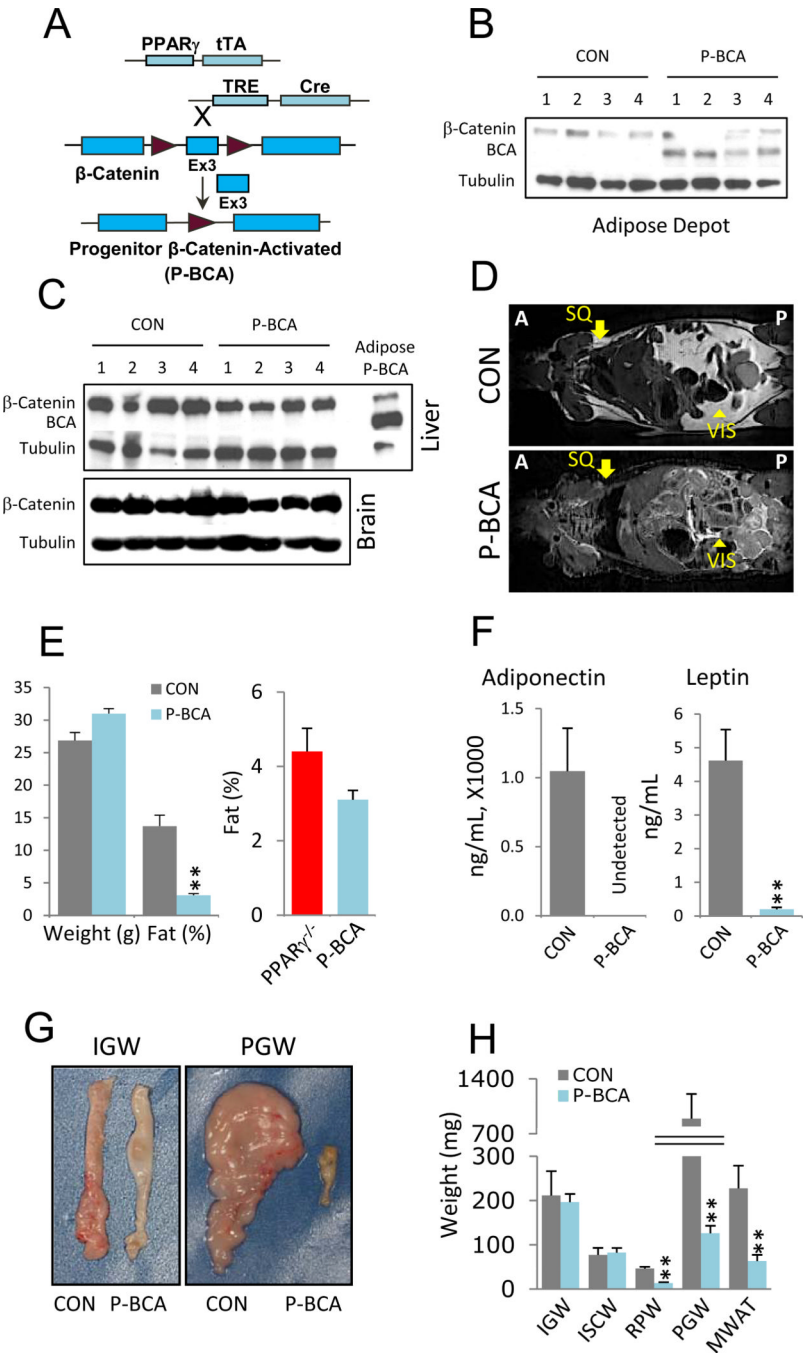

Figure 2. β-catenin Activation in Adipose Progenitors Reduces Adiposity

(A) Schematic of progenitor cell-autonomous activation of β-catenin (P-BCA) using a tet transactivator (tTA) knocked-into exon 2 of the PPARγ locus. In PPARγ positive cells, tTA is translated and binds to a transgenic tet-response element (TRE), inducing Cre expression and β-catenin activation. Maroon arrowheads represent LoxP sites.

(B, C) Westerns of control (CON) and P-BCA inguinal adipose depots (B) or livers and brains (C) assayed with anti-β-catenin and anti-tubulin antibodies. β-catenin indicates wild-type form; BCA indicates activated form. Tubulin serves as loading control. In C, P-BCA adipose depot extracts are a BCA positive control.

(D) MRI scans of control and P-BCA siblings. Arrows indicate normal location of subcutaneous (SQ) adipose depots; arrowheads indicate visceral (VIS) adipose depots. Anterior (A); Posterior (P).
(E) Left plots show weight and percent body fat (NMR spectroscopy), of control and P-BCA siblings. Right plot is percent body fat of PPARγ nulls ($PPAR\gamma^{-/-}$) and P-BCA mutants.
(F) Adiponectin and leptin levels of control and P-BCA sibling sera.
(G) Representative inguinal (IGW) and perigonadal (PGW) WAT explants of control and P-BCA siblings.
(H) Weights of various adipose depots, as in Figure 1G, of control and P-BCA siblings. Representative studies on 4-month old sibling males; n ≥ 8 per cohort, repeated ≥ 3 cohorts. Female data mirrored these effects elicited by the P-BCA mutation. Error bars indicate SEM. Statistical significance assessed by two-tailed Student's t-test, **p<0.01.

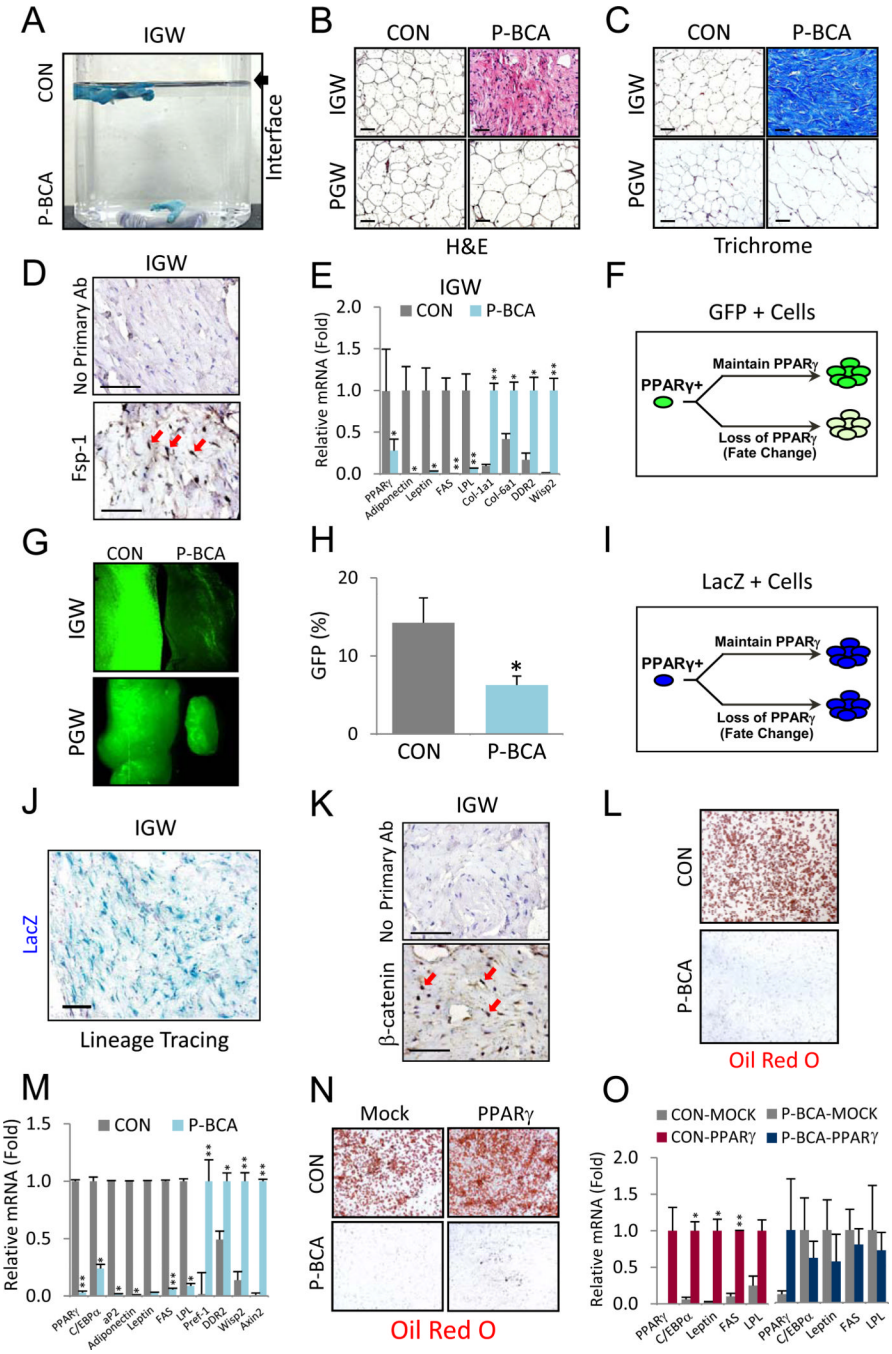

Figure 3. The P-BCA Mutation Induces a Lineage Change in Subcutaneous Adipose Tissue

(A) Photograph of control (CON) and P-BCA inguinal adipose depots (blue) in water. Arrow denotes air-water interface.

(B) Hematoxylin and eosin (H&E) stained histological sections of control and P-BCA IGW and PGW.

(C) Sections of control and P-BCA IGW and PGW stained with trichrome (collagen stains blue).

(D) Fibroblast specific protein-1 (Fsp-1) immunohistochemistry of P-BCA IGW. Top panel shows P-BCA IGW negative control without primary antibody. Fsp-1 stained dark brown (DAB); hematoxylin labels nuclei blue. Red arrows indicate some Fsp-1 positive cells.

(E) qPCR of control (CON) and P-BCA IGW for the indicated markers: PPARγ is an adipogenic transcription factor; adiponectin, Leptin, FAS and LPL are adipocyte markers; Col-1a1, Col-6a1 and DDR2 are fibroblast markers; Wisp2 is a Wnt target. n ≥ 6 per cohort, repeated ≥ 3 cohorts.
(F) Cartoon depicting PPARγ-dependent marking of cells using H2B-GFP (green) within PPARγ-positive (PPARγ+) lineage using the tet-transactivator system (tTA). PPARγ-tTA drives expression of TRE-H2B-GFP. If the cell lineage continues to express PPARγ, they and their descendants express GFP (green, top arrow path). If PPARγ expression is blunted, for example with a fate change, GFP expression is diminished (bottom arrow path).
(G) GFP-fluorescent images of P-BCA and sibling IGW and PGW.
(H) IGW SV cells were measured for percentage of GFP positivity (Y-axis) with flow cytometry. The GFP+ gates set based on controls with the TRE-H2B-GFP reporter alone. n ≥ 6 per cohort, repeated ≥ 3 cohorts.
(I) Illustration of PPARγ-dependent lacZ (blue) marking within PPARγ-positive (PPARγ+) lineage using the tTA. lacZ is an indelible marker in which Cre excises a transcriptional stop cassette within the Rosa26 lacZ reporter (R26R). Once a cell expresses PPARγ-tTA and Cre (from TRE-Cre allele), lacZ is permanently expressed, due to removal of the stop cassette 5' of the lacZ gene, regardless of PPARγ expression in the cells and all descendants.
(J) Sections of X-gal stained P-BCA IGW.
(K) β-catenin staining of P-BCA IGW sections. Top panel shows P-BCA IGW negative control without primary antibody. β-catenin stains dark brown (DAB); hematoxylin stains nuclei blue. Red arrows indicate β-catenin positive nuclei.
(L, M) SV cells of control and P-BCA sibling IGW were isolated, cultured and adipogenically induced. Adipogenesis was assayed with Oil Red O (L, fat stains red) and qPCR (M) of adipogenic (PPARγ, C/EBPα, aP2, Adiponectin, Leptin, FAS, and LPL), preadipocyte (Pref-1), fibroblast (DDR2), and Wnt target (Wisp2, Axin2) markers. n ≥ 6 per cohort, repeated ≥ 3 cohorts.
(N, O) SV cells were isolated from control and P-BCA siblings, infected with either empty or PPARγ retrovirus, and adipogenically induced. Adipogenesis was assayed with Oil Red O (N) and qPCR (O). In O, control (left graph) and P-BCA (right graph) IGW SVF infected with either mock or PPARγ virus: PPARγ and C/EBPα are adipogenic transcription factors; Leptin, FAS and LPL are adipocyte markers. n ≥ 6 per cohort, repeated ≥ 3 cohorts. Scale bar = 100μm. Error bars indicate SEM. Statistical significance assessed by two-tailed Student's t-test, *$p<0.05$, **$p<0.01$.

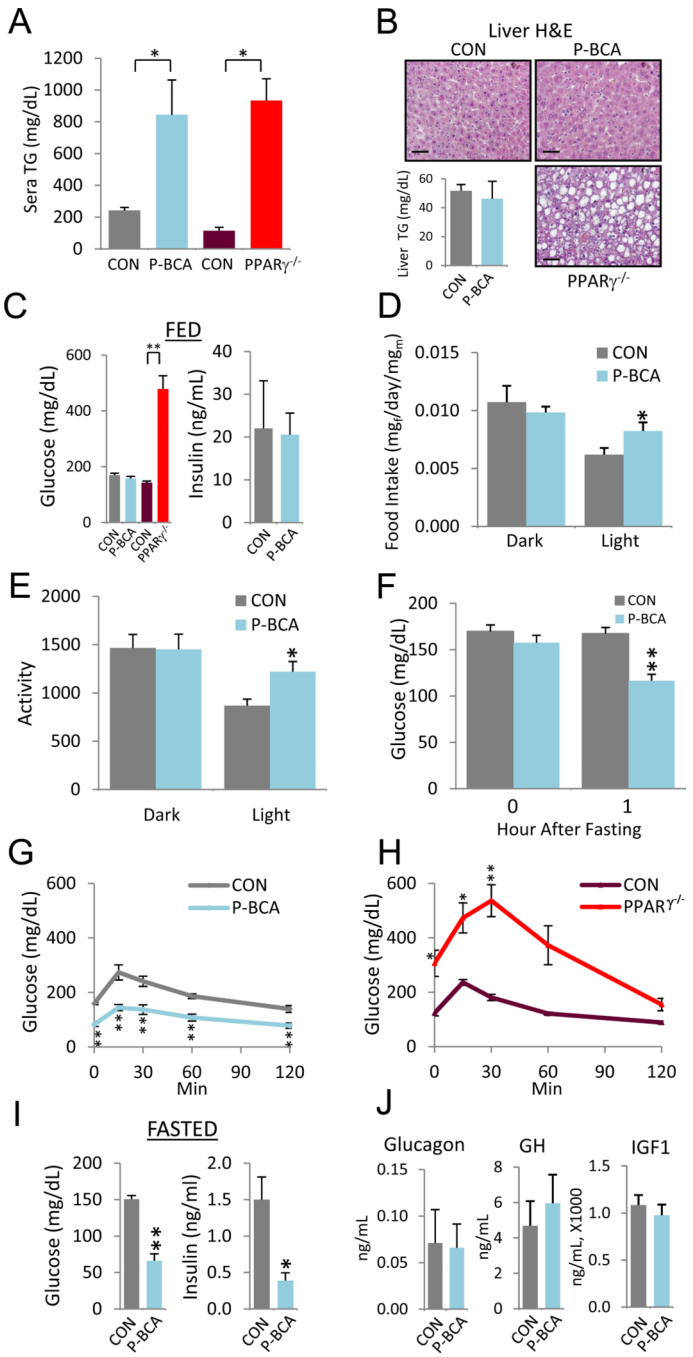

Figure 4. Paradoxically Improved Metabolism in Lipodystrophic P-BCA Mutants

(A) Serum triglyceride levels of control and P-BCA siblings, and control and PPARγ null (PPARγ$^{-/-}$) siblings. Significance compared to sibling control.

(B) H&E stained sections of control, P-BCA, and PPARγ null livers (top row and bottom right panel). Bar graph of triglyceride quantification of control and P-BCA liver extracts (bottom left panel).

(C) Random (FED) blood glucose (left) and serum insulin (right) levels of control and P-BCA sibling and control and PPARγ null sibling. Significance values compared to sibling control.

(D, E) Food intake (D; mg food/day/mg mouse) and activity (X-Y movement) (E) during dark and light cycles.
(F) Blood glucose levels of control and P-BCA siblings at beginning and 1 hour after food removal.
(G, H) GTT of control and P-BCA siblings (G) and control and PPARγ null siblings (H).
(I, J) Blood glucose (left) and serum insulin (right) levels (I) and sera glucagon, growth hormone (GH) and insulin-like growth factor-1 (IGF1) (J) of control and P-BCA siblings 4 hours after food withdrawal.
Representative studies on 4-month old sibling males; n ≥ 8 per cohort, repeated ≥ 3 cohorts. Female data mirrors these effects elicited by the P-BCA mutation. Scale bar = 100μm. Error bars indicate SEM. Statistical significance assessed by two-tailed Student's t-test, *$p<0.05$, **$p<0.01$

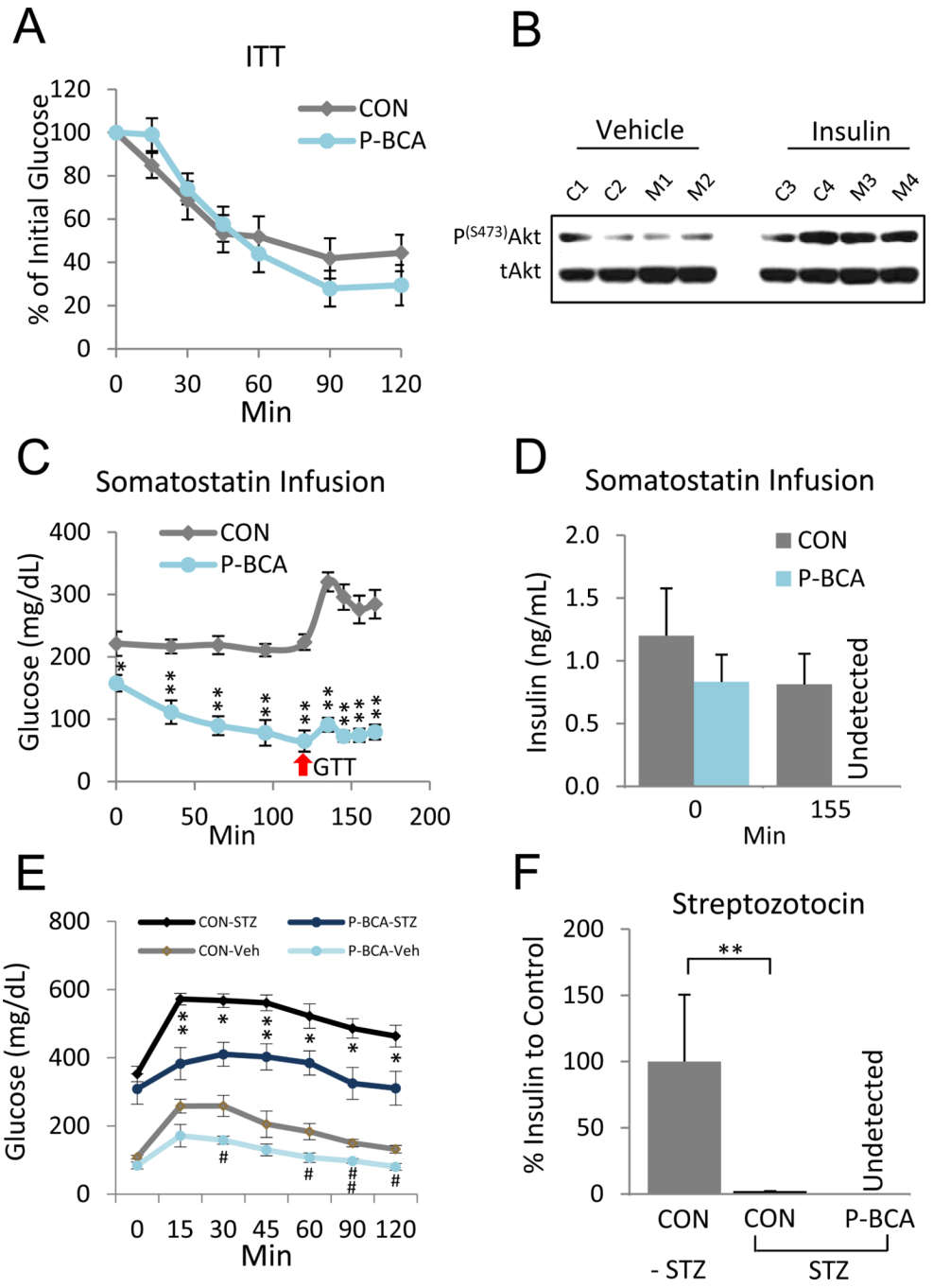

Figure 5.

P-BCA Hypoglycemic Phenotype is Not Due to Increased Insulin Sensitivity

(A) Insulin tolerance test (ITT) of control and P-BCA siblings. n ≥ 8 per cohort, repeated ≥ 3 cohorts.

(B) Akt Western analysis of gastrocnemius muscle extracts 15 minutes after control (C1-C4) and P-BCA mutant (M1-M4) mice were injected with either vehicle (left panel) or insulin (right panel). p = phosphorylated, t = total

(C, D) Glucose (C) and insulin (D) levels of control and P-BCA male siblings during somatostatin infusion. Somatostatin was infused at time 0. At 120 minutes (red arrow) a

bolus of glucose was injected with continued somatostatin infusion. Bar graph of insulin levels at times 0 and 155 minutes (D). n ≥ 10 per cohort, repeated ≥ 2 cohorts.
(E, F) GTT and insulin levels of vehicle and streptozocin (STZ)-treated control and P-BCA siblings three weeks after STZ administration. Insulin levels normalized to -STZ control. Significance values compared to respective controls without STZ treatment. n ≥ 8 per cohort, repeated ≥ 2 cohorts.
Error bars indicate SEM. Statistical significance assessed by two-tailed Student's t-test, * or # $p<0.05$, **or ## $p<0.01$.

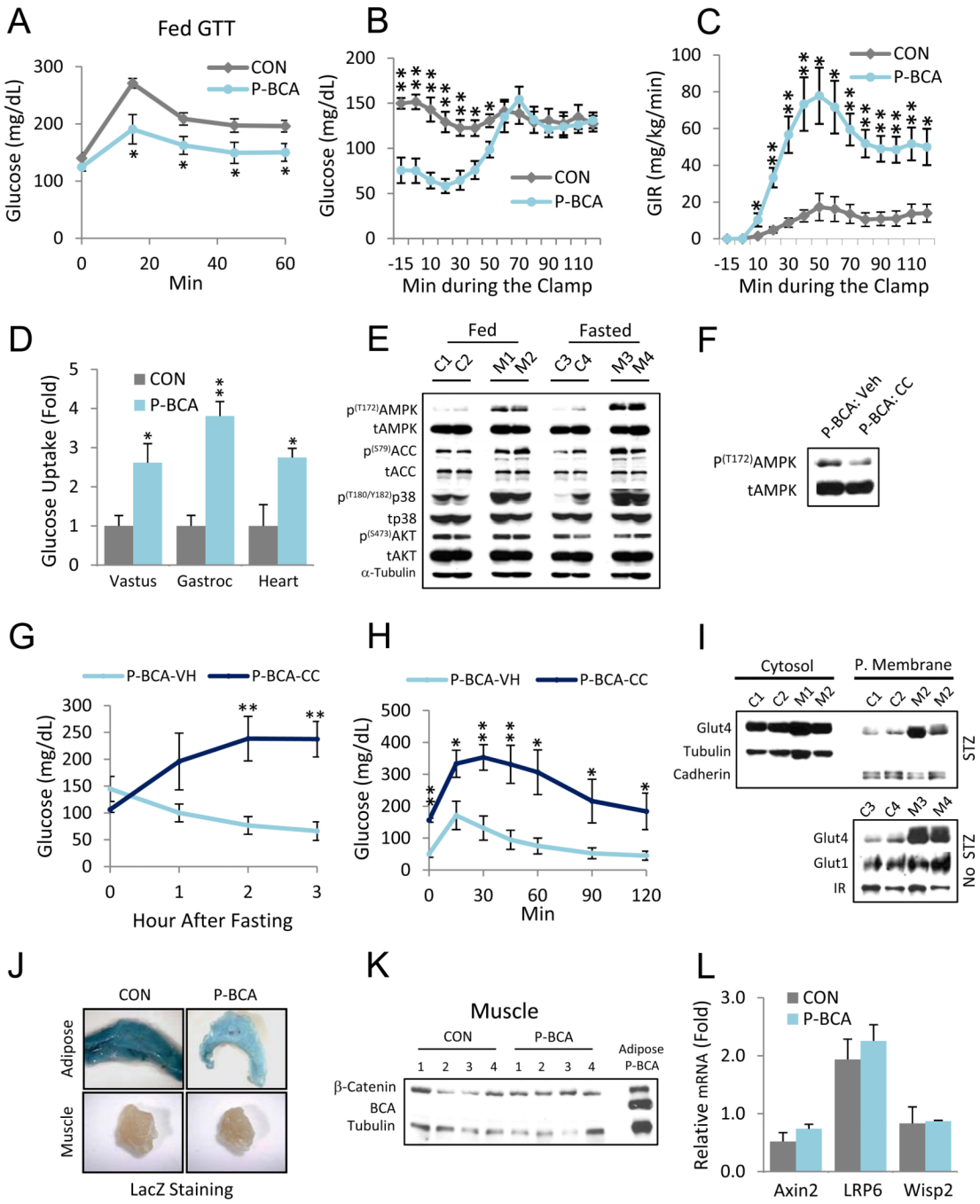

Figure 6. Increased Glucose Uptake in P-BCA Muscles with Activation of AMPK, but Not Wnt signaling

(A) Fed GTT of control and P-BCA mutant mice. n ≥ 8 per cohort, repeated ≥ 3 cohorts. (B, C, D) Hyperinsulinemic-euglycemic clamps of control and P-BCA siblings. Insulin and glucose infusions were started at time 0, 5 hours after food removal. (B) Blood glucose levels and (C) glucose infusion rate (GIR) 15 minutes before and during clamp. (D) Glucose uptake of indicated muscles (Vastus = vastus medialis, Gastroc = gastrocnemius) derived from isotope incorporation 30 minutes after injection of ^{14}C 2-deoxyglucose at time 120 minutes of clamp. n ≥ 10, repeated ≥ 2 cohorts.

(E) Western blots of proteins isolated from fed and fasted (4 hours) sibling 4-month old male gastrocnemius muscles probed with the indicated antibodies. C = control, M = P-BCA mutant, p = phosphorylated, t = total.
(F) AMPK blots of gastrocnemius muscles of P-BCA siblings injected with vehicle (P-BCAVeh) or Compound C (P-BCA-CC), p = phosphorylated, t = total.
(G) Fasting blood glucose levels of P-BCA males injected with vehicle (P-BCA-VH) or Compound C (P-BCA-CC). Mice were injected with vehicle or Compound C at time 0 then fasted for three hours.
(H) GTT of P-BCA males injected with vehicle (P-BCA-VH) or Compound C (P-BCA-CC) and fasted for four hours.
(I) Fractionation of cytoplasm and plasma membrane from limb muscles of control (C1-C4) and P-BCA (M1-M4) male siblings both with and without STZ. Cadherin and the insulin receptor (IR) are plasma membrane markers, tubulin is a cytoplasm marker.
(J) IGW and muscles of control (CON) and P-BCA mice were removed and incubated in X-gal. Blue color reflects lacZ expression.
(K) Western blot of muscle extracts of 4 control and 4 P-BCA siblings probed with anti-β-catenin and anti-tubulin antibodies. β-catenin indicates wild-type form; BCA indicates activated form. Tubulin serves as loading control. P-BCA adipose depot extracts are BCA positive control.
(L) qPCR of control and P-BCA muscle extracts for the indicated β-catenin targets. $n \geq 8$ per cohort, repeated ≥ 3 cohorts.
Error bars indicate SEM. Statistical significance assessed by two-tailed Student's t-test, *$p<0.05$, **$p<0.01$.

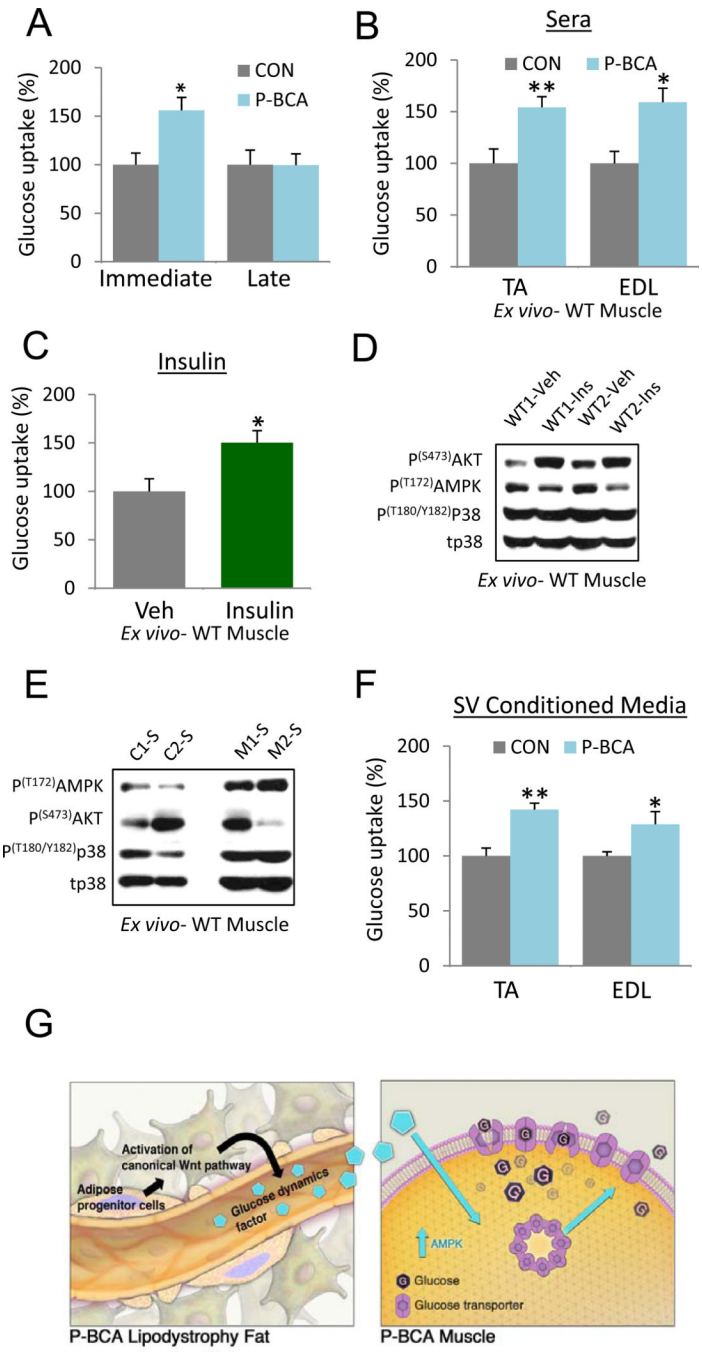

Figure 7. Serum-borne Factor Increases Glucose Uptake in Muscle

(A) *Ex vivo* glucose uptake assay of sibling control (CON) and P-BCA muscles either immediately after excision (left portion, immediate) or three hours after incubation in C57BL/6 (wild-type) serum (right portion, late). n ≥ 4 per cohort, repeated ≥ 2 cohorts.

(B, C) Glucose uptake of C57BL/6 (WT) TA and EDL muscle explants incubated for one hour in: sibling control (CON) or P-BCA sera (B) or C57BL/6 (WT) sera with vehicle (Veh) or insulin (Ins, 1U/ml) (C). n ≥ 4 muscles per cohort, n ≥ 3 sera per study, for control and P-BCA sera repeated ≥ 10 cohorts.

(D, E) Western blots of proteins isolated from C57BL/6 (WT) muscles incubated in WT sera with vehicle (WT1-Veh, WT2-Veh) or insulin (WT1-Ins, WT2-Ins, 1U/ml) (C) or in sibling

control (C1-S, C2-S) or P-BCA sera (M1-S, M2-S) (D) for 15 minutes and probed with indicated antibodies. p = phosphorylated, t = total.
(F) Glucose uptake of WT TA and EDL muscle explants (1–2 month old) incubated for one hour in conditioned media of SV cells derived from sibling control or P-BCA SQ adipose depots. n ≥ 4 muscles per cohort, n ≥ 3 conditioned media per cohort, repeated ≥ 3 cohorts.
(G) Model of P-BCA adipose tissue and muscle. P-BCA mice have increased glucose uptake in muscle, increased glucose transporters at the myocyte cell surface, and activated AMPK (blue arrows). The changes in muscle (e.g., increased glucose uptake, activated AMPK, etc.) are secondary to a non-autonomous signal, for example a factor (glucose dynamics factor, blue pentagon) secreted from the adipose stem cells in which β-catenin is activated.
Error bars indicate SEM. Statistical significance assessed by two-tailed Student's t-test, *p<0.05, **p<0.01.